

Three-dimensional magnetohydrodynamic simulations of M-dwarf chromospheres

S. Wedemeyer^{1,2,*}, H.-G. Ludwig³, and O. Steiner⁴

¹ Institute of Theoretical Astrophysics, University of Oslo, P.O. Box 1029 Blindern, N-0315 Oslo, Norway

² Center of Mathematics for Applications (CMA), University of Oslo, Box 1053 Blindern, N-0316 Oslo, Norway

³ ZAH, Landessternwarte Königstuhl, D-69117 Heidelberg, Germany

⁴ Kiepenheuer Institute for Solar Physics, Schöneckstrasse 6-7, D-79104 Freiburg, Germany

Received 2012 Jul 11, accepted 2012 Dec 5

Published online 2013 Feb 1

Key words stars: atmospheres, chromospheres, magnetic fields; convection, magnetohydrodynamics (MHD), radiative transfer, shock waves.

We present first results from three-dimensional radiation magnetohydrodynamic simulations of M-type dwarf stars with CO5BOLD. The local models include the top of the convection zone, the photosphere, and the chromosphere. The results are illustrated for models with an effective temperature of 3240 K and a gravitational acceleration of $\log g = 4.5$, which represent analogues of AD Leo. The models have different initial magnetic field strengths and field topologies. This first generation of models demonstrates that the atmospheres of M-dwarfs are highly dynamic and intermittent. Magnetic fields and propagating shock waves produce a complicated fine-structure, which is clearly visible in synthetic intensity maps in the core of the Ca II K spectral line and also at millimeter wavelengths. The dynamic small-scale pattern cannot be described by means of one-dimensional models, which has important implications for the construction of semi-empirical model atmospheres and thus for the interpretation of observations in general. Detailed three-dimensional numerical simulations are valuable in this respect. Furthermore, such models facilitate the analysis of small-scale processes, which cannot be observed on stars but nevertheless might be essential for understanding M-dwarf atmospheres and their activity. An example are so-called “magnetic tornadoes”, which have recently been found on the Sun and are presented here in M-dwarf models for the first time.



© 2013 WILEY-VCH Verlag GmbH & Co. KGaA, Weinheim

1 Introduction

Our picture of the atmospheric fine-structure of our Sun changed substantially during the past decades. Progress in instrumental performance resulted in unprecedented high-resolution observations that reveal a high degree of structure on a multitude of spatial and temporal scales. Such a complex phenomenon cannot be described in sufficient detail by means of otherwise elaborate semi-empirical one-dimensional model atmospheres (e.g. Vernazza et al. 1981). The importance of small-scale spatial and temporal variations in the solar chromosphere has been realized (cf. Ayres & Rabin 1996; Carlsson & Stein 1995; Solanki et al. 1991) and is now an essential feature of state-of-the-art numerical models. Furthermore, the layers of the Sun are no longer treated individually but as integral components of a dynamically coupled atmosphere (Wedemeyer-Böhm et al. 2009).

Here we present a new class of 3-D models for M-dwarf stars that clearly demonstrates that their atmospheres are dynamic and intermittent, too. This finding immediately gives rise to the question to what extent such inhomogeneities affect the emergent radiative intensity and related chromospheric diagnostics. In order to address this question, we

use model snapshots as input for spectrum synthesis calculations and discuss the resulting implications of the spatial and temporal inhomogeneities for the interpretation of observations and for the construction and usage of one-dimensional static model atmospheres.

2 Numerical simulations

The code. The numerical simulations are carried out with the 3-D radiation magnetohydrodynamics code CO⁵BOLD (Freytag et al. 2012). The code numerically solves the equations of (ideal) magnetohydrodynamics and radiative transfer together with a realistic equation of state and multi-group opacities. The simulation is advanced in time step by step and outputs a time sequence of 3-D snapshots and auxiliary data. CO⁵BOLD is applied to a large range of different stars, among them the Sun (Steiner et al. 2008; Wedemeyer et al. 2004) and red giants (Freytag et al. 2002). Wende et al. (2009) used CO⁵BOLD to calculate local hydrodynamic models of M-type dwarf stars, which all include the top of the convection zone and the photosphere for a few selected parameter sets of T_{eff} and $\log g$ (see also Beeck et al. 2011). The local simulations presented here include in addition a chromosphere and magnetic fields. The opacity tables are

* Corresponding author: e-mail: sven.wedemeyer@astro.uio.no



© 2013 WILEY-VCH Verlag GmbH & Co. KGaA, Weinheim

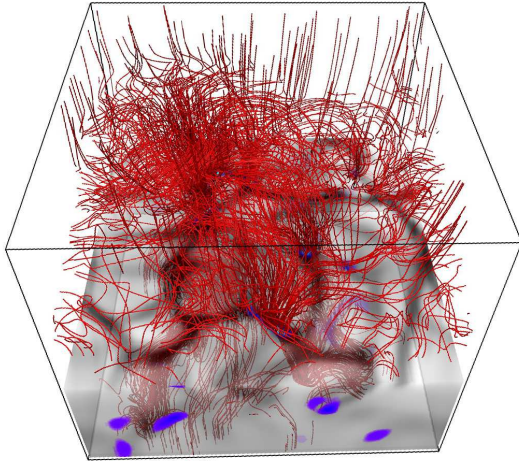


Fig. 1 Visualisation of a 3-D model snapshot for a M-dwarf model with $T_{\text{eff}} = 3240$ K, $\log g = 4.5$, and an initial magnetic field strength of $|B|_0 = 100$ G (2×2 checkerboard). The bottom of the photosphere and the convection zone are grey-shaded, whereas regions of high magnetic field strength are coloured bluish. The red lines represent magnetic field lines. This image was produced with VAPOR (Clyne et al. 2007; Clyne & Rast 2005).

based on PHOENIX NextGen data (Hauschildt et al. 1999). A particular challenge is that the typical computational time step for M-dwarf chromosphere models is on the order of only 1 ms, owing to the short time scales in the magnetized chromosphere.

The models. A systematic model grid for different types of M-dwarf stars is currently under production. Here, we present exemplary models with $T_{\text{eff}} = 3240$ K and $\log g = 4.5$, which represent (weak-field) analogues of AD Leo. The models have a horizontal extent of $1950 \text{ km} \times 1950 \text{ km}$ and reach from -700 km in the convection zone to $+1000$ km in the chromosphere. All models start from a hydrodynamic simulation snapshot that has been relaxed from its initial conditions. The initial magnetic field, which is superimposed on the hydrodynamic model, is either unipolar and vertical or consists of regions of vertical field with opposite polarity (2×2 checkerboard). The individual models have initial magnetic field strengths ranging from 10 G to 500 G.

3 Atmospheric structure and dynamics

Under the conditions in the low photosphere outside strong magnetic flux concentrations (i.e., in quiet regions), the magnetic field is effectively "frozen-in". Consequently, the flow field generated by the surface convection continuously rearranges the magnetic field – like on the Sun. The initial magnetic field is swept into the intergranular lanes, where it is concentrated in form of continuous sheets and knots. Especially in lane vertices, this process produces magnetic

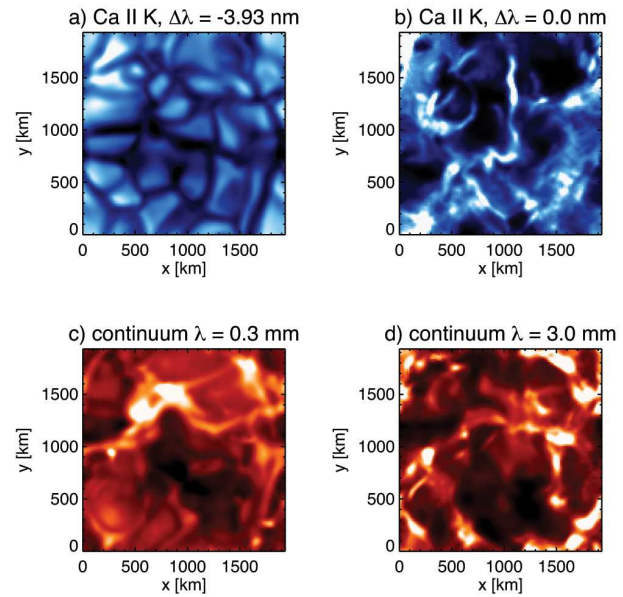


Fig. 2 Synthetic intensity images for a selected model snapshot. *Top*: Ca II K line wing (left) and line core (right). *Bottom*: continua at 0.3 mm (left) and 3.0 mm (right).

flux concentrations with field strengths in excess of 1 kG. The initial field is thus quickly transformed into a complicated non-uniform field. The complex geometry cannot sufficiently be described as a set of idealized "flux tubes".

The magnetic field expands from these photospheric footpoints into the chromosphere, where it funnels out and fills the whole volume. The chromospheric magnetic field nevertheless exhibits a fine-structure that varies on short time scales. In the mixed polarity runs, magnetic loops form which connect footpoint areas of opposite polarity. The resulting 3-D structure consists of entangled field lines which are often twisted and rapidly change in time (see Fig. 1). As a consequence, the model chromosphere varies strongly in space and time, resulting in strong variations in the physical state of the atmospheric plasma. Like for the Sun, a broad distribution of gas temperatures is found in the upper layers. While upwards propagating shock fronts produce high temperature peaks in the chromosphere, the plasma in the post-shock regions cools to low temperatures. This non-uniform temperature distribution has to be taken into account when calculating meaningful average atmospheric stratifications.

4 Synthetic intensity maps

We illustrate the consequences of the complex atmospheric structure for the interpretation of observations. To this aim, we apply radiative transfer codes to three model snapshots for generating synthetic intensity maps, which can be interpreted as virtual observations of the model.

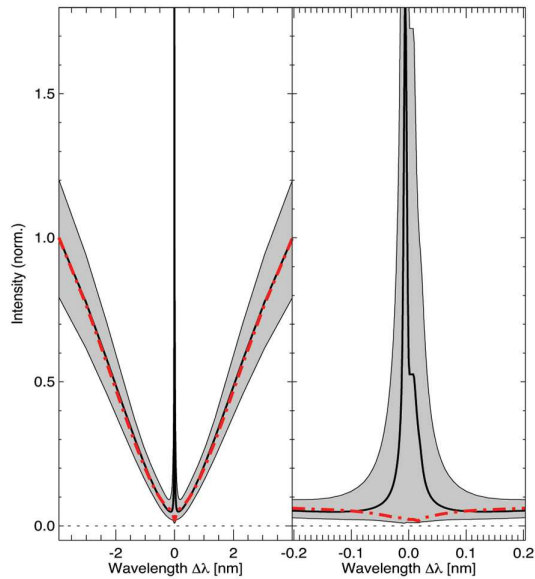


Fig. 3 Synthetic intensity profiles of the Ca II K spectral line for a selected 3-D model snapshot. *Left:* The whole line profile. *Right:* Close-up of the line core. The grey area between the 1 and the 99 percentiles marks the value range covered by the majority of the individual locations in the model. The corresponding 3-D average (thick black line, averaged horizontally over all columns in the 3-D model) exhibits a central emission peak. In contrast, the horizontally averaged model, i.e. the corresponding 1-D mean atmosphere, results in a spectral line profile with no emission peak (red dot-dashed line).

Calcium. First, we use MULTI3D (Carlsson 1986), which provides the detailed solution of the radiative transfer equation in non-LTE (non-local thermodynamic equilibrium). The output contains intensity cubes ($I = f(x, y, \lambda)$) for 5 spectral lines (Ca II H, K, IRT) for each selected snapshot. Exemplary intensity maps in the line wing and in the line core are shown in Fig. 2. The line wing image essentially shows the granulation pattern originating from the low photosphere. The scene is completely different in the line core image. The interplay of magnetic fields and propagating shock waves causes an intermittent pattern of bright filamentary threads and dark regions, which mostly correspond to hot shock fronts and cool post-shock regions, respectively. The spectral line profiles accordingly vary significantly for the different locations. The intensity range covered by the individual Ca II K lines profiles is illustrated in Fig. 3. Despite the large spatial variations, the spatially averaged line profile still exhibits a strong central emission reversal peak. For comparison, the model snapshot has been averaged horizontally, resulting in a one-dimensional model atmosphere. When computing the Ca II K line profile from this 1-D model atmosphere, again using MULTI3D, it does not show a central emission peak, which is in strong contrast to the full 3-D result. Similar 1-D average atmospheres for other model snap-

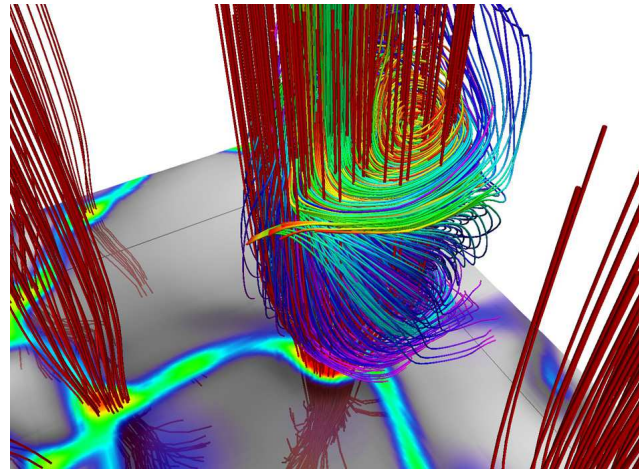


Fig. 4 Visualisation of a 3-D model snapshot for a M-dwarf model with $T_{\text{eff}} = 3240$ K, $\log g = 4.5$, and an initial vertical magnetic field strength of $|B|_0 = 100$ G (2×2 checkerboard). The absolute magnetic field strength is color-coded in a plane that represents the bottom of the photosphere. The magnetic field lines (red) are concentrated in the intergranular lanes and funnel out in the atmosphere above. The plasma in the chromosphere follows the rotating magnetic field structures, resulting in spiral trajectories (green-blue lines). It is the first time that such a “magnetic tornado” has been found in a model of a cool star.

shots can show emission in the line core but the differences to the 3-D result are always significant. It demonstrates that spatial averaging removes the strong fluctuations connected to the dynamic small-scale structure in the model chromosphere, resulting in synthetic spectral line profiles that carry only limited if not misleading information.

(Sub-)millimeter continua. The continuum intensity at (sub-)millimeter wavelengths is another promising way to map the chromospheric layers. The large diagnostic potential has been demonstrated for the Sun (Wedemeyer-Böhm et al. 2007). We use the radiative transfer code LINFOR3D (M. Steffen, http://www.aip.de/~mst/linfor3D_main.html) to calculate the continuum intensity for wavelengths between 0.3 mm and 9.0 mm, which lie in the range observable with the Atacama Large Millimeter Array (ALMA). Two exemplary intensity maps are shown in Fig. 2. The average height in the atmosphere, where the intensity is formed, increases with increasing wavelength. For a plane-parallel stratified atmosphere, it would essentially map different chromospheric layers at the different wavelengths. However, the intermittent atmospheric structure results in large differences in the effective formation height range. At the same wavelength, it is possible to see deeper into the atmosphere at certain locations than at others. The effective formation height range thus varies spatially and temporally and may make it difficult to derive a meaningful atmospheric stratification from disk-averaged continuum intensity observations.

5 Implications for one-dimensional models

Fuhrmeister et al. (2005) provide a semi-empirical model atmosphere for AD Leo, in which the gas temperature first decreases with height in the photosphere and increases essentially linearly in the chromosphere, followed by a characteristic jump in the transition region. The range of temperatures found in our 3-D model photosphere and with it the corresponding average match the stratification by Fuhrmeister et al. (2005) quite well since the temperature fluctuations are only moderate in that layer. The temperature range drastically broadens in the 3-D model chromosphere, owing to the onset of shock formation. Peak temperatures on the order of 5500 K are found in many locations throughout the chromosphere, resulting in a height-dependent distribution that overlaps with the semi-empirical model. The arithmetic horizontally averaged temperature, however, increases only mildly with height because hot and cold regions cancel. The temperature stratification obviously depends on how the temperatures enter the average. The relation between (local) gas temperature and emergent intensity can be strongly non-linear for many spectral lines that are formed in the chromosphere, incl. the lines of Ca II. Deriving a one-dimensional temperature stratification from spatially unresolved spectra can thus effectively lead to a higher weighting of the high temperatures connected to shock fronts.

Additional complications include largely varying formation height ranges, which makes it difficult to assign a definite height to an empirically derived temperature value. Consequently, the question arises how meaningful such 1-D average stratifications are.

6 Small-scale dynamics

Numerical simulations serve as a tool for analyzing and predicting physical processes. The Sun plays an important role as a reference. The applied numerical methods can be tested by detailed comparisons of solar models with spatially resolved observations of the Sun. For cool stars, adjustments and additional physics may be needed but nevertheless there are many qualitative similarities between solar and stellar models. A recent example are so-called magnetic tornadoes on the Sun (Wedemeyer-Böhm et al. 2012). They are generated by the interplay of magnetic fields and vortex flows in the photosphere of the Sun. These vortex flows develop due to the conservation of angular momentum of cooled plasma in the downdrafts near the surface. In magnetically quiet Sun regions, the magnetic field is advected with the photospheric flows, which forces the magnetic footpoints to rotate. The magnetic field mediates the rotation into the upper layers, where the situation reverses and the plasma follows the rotating field, resulting in spiral trajectories. The net energy transport associated with these tornado-like events may significantly contribute to the heating of the solar corona.

The models presented here suggest that photospheric vortex flows are abundant on the surface of cool M-dwarfs,

too, like it was already found by Ludwig et al. (2002, 2006). As on the Sun, they force the magnetic footpoints to rotate and thus generate magnetic tornadoes in the chromosphere above. An example is illustrated in Fig. 4. It is plausible that these small-scale tornadoes are common on M-dwarf stars, too, which could be of importance for the energy balance of their outer atmospheric layers.

7 Conclusions

Already the first model generation clearly demonstrates that M-dwarf atmospheres are very dynamic and highly structured on small spatial and temporal scales. Consequently, a detailed 3-D treatment is required for a realistic description. One-dimensional model atmospheres, which are constructed from a comparison to observed spectra, reproduce certain features but, by nature, cannot account for important properties of the atmospheres. Nevertheless, detailed 1-D models will remain complementary to 3-D models until all required physical processes can be treated numerically in sufficient detail. Such advanced 3-D models will be essential for understanding the magnetic activity of M-type dwarf stars.

Acknowledgements. This work was supported with a grant of the Research Council of Norway (No. 208011/F50, “Magnetic Activity of the Atmospheres of M-type Dwarf Stars”).

References

- Ayres, T. R. & Rabin, D. 1996, ApJ, 460, 1042
- Beeck, B., Schüssler, M., Reiners, A. 2011, In Johns-Krull, Browning, West (Eds.), ASP Conf. Series, Vol. 448, 1071
- Carlsson, M. 1986, Uppsala Astronomical Observatory: Report No. 33
- Carlsson, M. & Stein, R. F. 1995, ApJ, 440, L29
- Clyne, J., Mininni, P., Norton, A., & Rast, M. 2007, New J. Phys, 9, 301
- Clyne, J. & Rast, M. 2005, in Proceedings of Visualization and Data Analysis 2005, Eds. Erbacher, R., Roberts, J.; Gröhn, M.; Börner, K., 284-294
- Freitag, B., Steffen, M., & Dorch, B. 2002, AN, 323, 213
- Freitag, B., Steffen, M., Ludwig, H.-G., et al. 2012, Journal of Computational Physics, 231, 919
- Fuhrmeister, B., Schmitt, J. H. M. M., & Hauschildt, P. H. 2005, A&A, 439, 1137
- Hauschildt, P. H., Allard, F., & Baron, E. 1999, ApJ, 512, 377
- Ludwig, H., Allard, F., & Hauschildt, P. H. 2002, A&A, 395, 99
- Ludwig, H.-G., Allard, F., & Hauschildt, P. H. 2006, A&A, 459, 599
- Solanki, S. K., Steiner, O., & Uitenbroeck, H. 1991, A&A, 250, 220
- Steiner, O., Rezaei, R., Schaffenberger, W., & Wedemeyer-Böhm, S. 2008, ApJ, 680, L85
- Vernazza, J. E., Avrett, E. H., & Loeser, R. 1981, ApJS, 45, 635
- Wedemeyer, S., Freitag, B., Steffen, M., Ludwig, H., & Holweger, H. 2004, A&A, 414, 1121
- Wedemeyer-Böhm, S., Lagg, A., & Nordlund, Å. 2009, Space Sci. Rev., 144, 317

- Wedemeyer-Böhm, S., Ludwig, H. G., Steffen, M., Leenaarts, J., & Freytag, B. 2007, *A&A*, 471, 977
- Wedemeyer-Böhm, S., Scullion, E., Steiner, O., et al. 2012, *Nature*, 486, 505
- Wende, S., Reiners, A., & Ludwig, H. 2009, *A&A*, 508, 1429